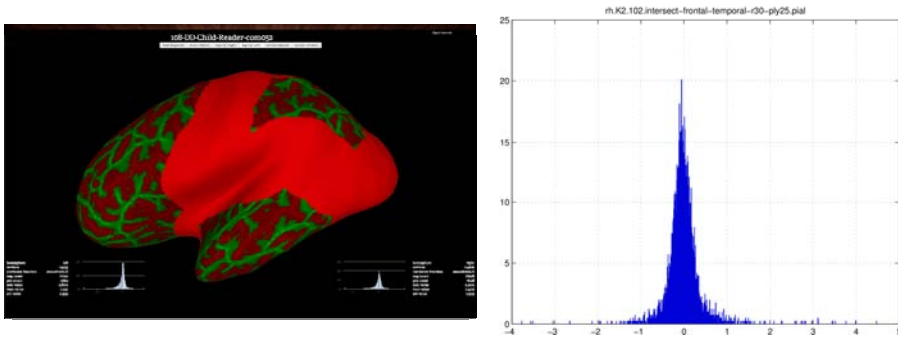


# Cuvature-based biomarkers for dyslexia: T1-image based surface analysis shows statistically separable dyslexic features

Rudolph Pienaar<sup>1,2</sup>, Kiho Im<sup>3,4</sup>, Mathieu Dehaes<sup>3,4</sup>, Sara Smith<sup>5</sup>, Barbara Peysakhovic<sup>5</sup>, Bryce Becker<sup>5</sup>, Nora Raschle<sup>5</sup>, P Ellen Grant<sup>1,2</sup>, and Nadine Gaab<sup>4,5</sup>

<sup>1</sup>Radiology, Children's Hospital Boston, Boston, MA, United States, <sup>2</sup>Radiology, Harvard Medical School, Boston, MA, United States, <sup>3</sup>Newborn Medicine, Children's Hospital Boston, Boston, MA, United States, <sup>4</sup>Pediatrics, Harvard Medical School, Boston, MA, United States, <sup>5</sup>Developmental Medicine, Children's Hospital Boston, Boston, MA, United States

**INTRODUCTION:** Robust cortical-based biomarkers for developmental dyslexia (DD) can provide meaningful insight into the patho-physiological development of the disorder, as well as providing the basis for improved understanding of its morphological characteristics. In this work we move beyond typical gray matter voxel-based morphometry and present results from a detailed curvature-based analysis, collected over automatically generated regions of interest from T1 weighted images in developmental dyslexia (DD) adults and children, typical (TYP) adults and children, and pre-reader children with a family history of dyslexia (FHD). The distribution of several different curvature functions (both intrinsic and extrinsic) are considered over the ROIs, collapsed down to single 2D points, and the clustering properties of these cumulative 2D clouds between different groups examined. We found statistically significant separation between dyslexic and non-dyslexic subjects based on curvature clustering of cortical surface properties.



**Figure 1:** Automatic ROI generation based on borders between lobar regions (on left); histogram of specific curvature function taken across a single ROI.

**METHODS:** T1-weighted MPRAGE MRI sequences were acquired on a Siemens 3T whole body scanner: 128 slices, TR 2000 ms; TE 3.39 ms; flip angle 9°; field of view 256 mm; voxel size 1.3×1.0×1.3 mm. Five groups of subject were considered *a priori*: **Group 1**, DD-Adults (6 subjects, ages 22y → 29y); **Group 2**, DD-Children (15 subjects, ages 7y → 12 y); **Group 3**, TYP-Adult (6 subjects, ages 20y → 30y); **Group 4**, TYP-Children (55 subjects, ages 5y → 12 y); and **Group 5**, FHD-Children (24 subjects, ages 5y → 10y). For each subject, ROIs were generated from FreeSurfer surfaces by finding a 2.5cm strip on each side of a border region between lobar regions. The

following ROIs were defined: frontal-parietal, frontal-temporal, parietal-occipital, parietal-temporal, temporal-occipital, which taken together paint a band as shown in Figure 1 (left). The curvature analysis considered for each region for each subject the histogram distribution (Figure 1 (right)) of curvature function values, where the curvature function  $c \in \{k_1, k_2, K=k_1k_2, H=\frac{1}{2}(k_1+k_2), S=(k_1-k_2)^2, B=k_1^2+k_2^2, C=\sqrt{B}\}$  and  $k_1$  and  $k_2$  are the principal curvatures calculated at each mesh vertex point. Cortical thickness at each mesh is also considered in this analysis. Each histogram plot was reduced to a single point for its positive and negative curvature lobes – this single point being the geometric centroid of the given signed curvature distribution. This essentially characterized each spread function with a signed mean value weighted by the expected occurrence of this mean. The set of all centroid points for all subjects was then grouped together, and some simple clustering performed. All the centroids for a given class on each region were again averaged, and a 2D standard deviation calculated in the mean and occurrence directions. These regions were examined for clean separation, and all classes that separated at this first-deviation border were deemed to show statistical group differences.

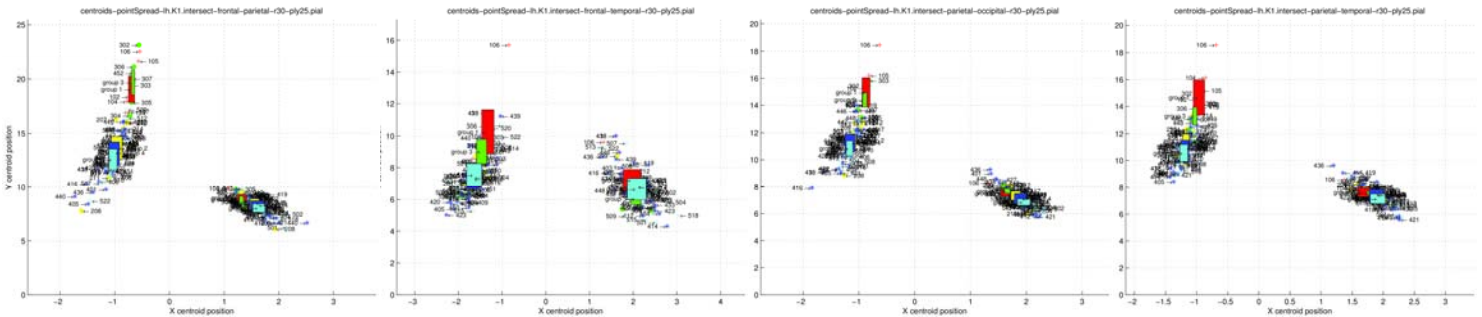


**Figure 2:** Curvature derived centroid clouds across the five cohort groups and across lobar border ROIs considered in this analysis: 1, DD-Adult: Red; 2, DD-Child: Yellow; 3, TYP-Adult: Green; 4, TYP-Child: Blue; 5, FHD-Child: Cyan.

| ROI-curv     | grp:1-2 | grp:1-3 | grp:1-4 | grp:1-5 | grp:2-3 | grp:2-4 | grp:2-5 | grp:3-4 | grp:3-5 | grp:4-5 |
|--------------|---------|---------|---------|---------|---------|---------|---------|---------|---------|---------|
| par-temp-k1  | 00.00   | 37.02   | 00.00   | 00.00   | 00.00   | 57.45   | 28.63   | 00.00   | 00.00   | 64.74   |
| par-occip-k2 | 00.00   | 00.00   | 00.00   | 00.00   | 00.00   | 43.06   | 42.25   | 00.00   | 00.00   | 81.63   |

**Table 1:** Percentage overlap between regions of significance for negative curvatures; columns denote percentage overlap between all combinations of clouds taken two at a time. The  $k_1$  result was on the smoothwm surface, the  $k_2$  on the pial.

**RESULTS:** The plots above show the 2D centroid clouds and the regions of cloud statistical significance for a single curvature function (here, the  $k_1$  principal curvature) on the left hemisphere across all the intersection ROIs taken on the pial surface. Note that the full analysis considers the set of all the curvature functions on both hemispheres for both the smoothwm and pial surface for each ROI, resulting in a space of 10,176 cluster sets. A visual inspection of the above plot quickly reveals some emergent properties that are conserved across all  $k_1$  curvature clouds: negative curvature values (corresponding to gyral shapes) show different and more separable clustering characteristics than positive (corresponding to sulcal troughs). Moreover, the DD clouds (Red – DD-Adult and Yellow DD-Child) group differently to the normals: DD- Adults and Children seem to have a higher mean  $k_1$  curvature than comparative Typical. Note also that the Adults (both DD and TYP) cluster together as a group separately to the Children. In fact, when examined over the entire space of all curvature functions, hemispheres, and surfaces, the left hemisphere showed the most significant difference between normal and dyslexic populations, with the parietal-temporal ROI and the parietal-occipital ROI showing the most consistent separation between regions (Table 1).

**CONCLUSION:** In this work we report initial results on a curvature-based analysis of cortical surfaces, and demonstrate that surface morphological differences can be quantified between normal and dyslexic groupings of adults and children. The ability for curvature-based surface measures to statistically characterize dyslexia can provide the basis for early intervention in cases where a dyslexic outcome is highly indicated.